Initiation and growth of the discontinuous precipitation reaction at [0 1 1] symmetric tilt boundaries in Cu Be alloy bicrystals

Initiation and growth of the discontinuous precipitation reaction at [011] symmetric tilt boundaries in Cu-Be alloy bicrystals

R. Monzen*, C. Watanabe, D. Mino and S. Saida

Department of Mechanical Systems Engineering, Kanazawa University,
2-40-20 Kodatsuno, Kanazawa 920-8667, Japan

Abstract

The initiation and growth of discontinuous precipitation (DP) at [011] symmetric tilt boundaries in Cu–0.75 wt% Be alloy bicrystals have been studied. Transmission electron microscopy revealed that γ precipitates tended to nucleate at a boundary in such a manner that their habit plane, $\{112\}_\alpha$ or $\{445\}_\alpha$, with one of the adjoining grains lay as close as possible to the boundary. The habit plane with a low energy formed on both sides of the precipitates behind an initially migrating boundary, indicating the importance of the existence of the low-energy habit plane for the initial boundary migration. The incubation period to initiate DP and cell growth rate for a boundary show a good correlation with the energy of the boundary. A kinetic analysis of DP using the models of Turnbull and Petermann and Hornbogen has yielded boundary diffusion data. A higher-energy boundary has a higher diffusivity with a smaller activation energy.

Keywords: Transmission electron microscopy; Copper alloy; Cellular growth; Coincidence lattice; Grain boundary migration

*Corresponding author. Fax: +81-76-234-4679. E-mail address: monzen@t.kanazawa-u.ac.jp (R. Monzen).

1. Introduction

The grain-boundary discontinuous precipitation (DP) reaction involves two critical steps, namely heterogeneous boundary precipitation and concurrent boundary migration. This results in a lamellar aggregate consisting of the precipitated phase and the solute-depleted matrix phase which are not in complete equilibrium regarding the chemical composition. The moving grain boundary, termed reaction front, provides a short-circuit path of solute transport [1].

In previous articles, we have studied systematically the formation and growth of DP at various [001] symmetric tilt [2] and twist [3] boundaries in orientation-controlled bicrystals of a Cu–0.75wt%Be alloy. For both types of boundaries, we have found that the incubation period for the cell formation and the cell growth rate at a boundary show a good correlation with the energy of the boundary. That is, higher-energy boundaries have a shorter incubation period and a faster growth rate. Furthermore, the grain-boundary diffusion data have been determined through the kinetic analysis of DP using the models of Turnbull [4] and Petermann and Hornbogen [5]. The activation energy and pre-exponential factor of grain-boundary diffusion versus misorientation curves display several peaks and the positions of these peaks are in agreement with those of cusps in the boundary energy versus misorientation diagram.

In this work, as an extension of these studies, the formation and growth of DP cells are investigated for [011] symmetric tilt boundaries in Cu–0.75wt%Be alloy bicrystals. The values of the activation energy and pre-exponential factor for boundary diffusion are also estimated as a function of the misorientation angle. In addition, the present article concerns the crystallography and morphology of the precipitated phase at grain boundaries and behind advancing boundaries, particularly in the initial stage of the DP reaction. Although the morphology and kinetics of DP in Cu–Be alloys have been investigated by several researchers [6-9], few detailed crystallographic aspects of DP have been studied by transmission electron microscopy (TEM).

The DP cell in Cu–Be alloys consists of lamellae of equilibrium γ (CuBe intermetallic) and depleted α (Cu-rich solid solution). The first critical step of the reaction is

heterogeneous grain-boundary nucleation. Bonfield and Edwards [10] have shown that in a Cu–Be–Co alloy the discontinuous precipitate designated as γI, which is nucleated at grain boundaries and grows into adjoining grains, has the same structure, lattice parameter and orientation as the continuously precipitated γ' intermediate precipitate. It has also been found that after extensive aging treatment at 425˚C, a transformation to the equilibrium precipitate γ occurs. Baumann *et al*. [9] have shown that at low temperatures (below about 500˚C) γ precipitates at a boundary initially nucleated induce boundary motion in a manner similar to, but differing in sequence from, the pucker mechanism of Tu and Turnbull [11, 12] in the initial stage of DP. Rioja and Laughlin [13] have reported that the γ' phase corresponding to γI forms as a DP reaction with the same orientation with the matrix as shown by Bonfield and Edwards [10].

2. Experimental procedure

Cu–0.75wt%Be alloy ingots were prepared by melting of electrolytic Cu (99.99%) and Cu–2.0wt%Be master alloy in a high-purity alumina crucible under an Ar atmosphere. Sheet-shaped bicrystals of this alloy, 2-mm thick, containing various [011] symmetric tilt boundaries with misorientation angles θ=16–153˚ were grown in a high-purity graphite mold by the Bridgman method using two seed crystals for each. Hereafter, the bicrystal with the misorientation angle θ and its grain boundary will be expressed as θ bicrystal and θ boundary, respectively. After confirming by the X-ray Laue analysis that the actual misorientation angles were within ±1˚ of the given angles, the bicrystals were homogenized at 850˚C and then spark-cut into specimen pieces of 1mm×15mm×15mm. The specimens were solution-treated at 800˚C for 1h in a vacuum, quenched into iced water and then aged at 300–400˚C for times up to 1440h in a vacuum. A chemical analysis showed that the aged specimens contained 0.75±0.01wt%Be.

Quantitative metallographic measurements were performed by optical microscopy. The interlamellar spacing λ was determined by the method previously reported by Tsubakino *et al*. [8, 14], as in previous studies [2, 3]. The foils for TEM were thinned at 5V in a twin-jet

electropolisher using a 20% solution of phosphoric acid in water at about 5˚C. Microscopy was carried out using a HITACHI H-9000NAR operating at 300 kV.

3. Results and Discussion

3.1. Crystallography of discontinuous precipitates

Although only the bicrystals with flat grain-boundaries before aging were used, the grain boundaries were curved when examined under TEM before the occurrence of DP. However, the deviations of the average grain-boundary planes from the pure tilt configuration were less than 10^{o}.

Grain-boundary precipitation took place before any significant boundary migration, similar to the observation of Baumann *et al*. [9]. Fig. 1 (a) shows a TEM image of precipitates at a θ=130˚ boundary after aging at 400˚C for 60h. Figs. 1(b), (c) and (d) are the $[011]_{\alpha}$ selected-area diffraction pattern (SADP) corresponding to (a), the schematic illustration of the previous SADP and the pertinent information given stereographically. In Fig. 1(c), the $[\bar{1}1\bar{1}]_{\alpha}$ direction in grain A is about 3˚ away from $[110]_{\gamma}$. An approximate orientation relationship between the Cu matrix of grain A and the precipitates can thus be stated as:

$$[011]_{\alpha}// [001]_{\gamma}; (\bar{3}1\bar{1})_{\alpha}//(130)_{\gamma},$$

in agreement with those for continuous precipitation reported by Shimizu *et al*. [15] and for DP reported by Bonfield and Edwards [10] and Rioja and Laughlin [13]. Most precipitates on grain boundaries aligned approximately with one of the adjacent grains according to this orientation relationship. Also we rarely observed the following orientation of precipitates:

$$[011]_{\alpha} // [001]_{\gamma}; (\bar{2}1\bar{1})_{\alpha}//(120)_{\gamma},$$

in agreement with that between a phase termed γ' and Cu matrix, reported by Geisller *et al*. [16]. Hereafter, the former or latter orientation will be expressed as orientation I or II. An example for orientation II is given in Fig. 2(b) where the angle between the $[\bar{1}1\bar{1}]_{\alpha}$ and $[110]_{\gamma}$ is about 1.5˚. The morphology of the precipitates giving rise to the extra reflections in Fig.

2(b) is shown in Fig. 2(a). It is seen that grain-boundary migration occurs. This will be discussed later. On the other hand, plate-shaped precipitates left behind advancing grain boundaries had the orientation relationship I to the Cu matrix (Fig. 3).

From analyses of the SADPs of Figs. 1(b) and 2(b) the boundary precipitates are found to have the lattice parameter a=b=0.27 nm, which is in accordance with that, a=0.27 nm, for the equilibrium phase γ with the B2 structure [16]. The plate-shaped precipitates also had the same lattice parameter. That the phase of the boundary precipitates and plate-shaped precipitates is γ was confirmed from the SADP in Fig. 3(b), in addition to those in Figs. 1(b) and 2(b). The precipitate in Fig. 3(a) exhibits the orientation relationship, $[01\bar{1}]_\alpha//[001]_\gamma$; $(311)_\alpha//(130)_\gamma$, to the Cu matrix, as seen in the stereographic projection in Fig. 3(c). An analysis of the SADP indicates that the precipitate has the lattice parameter b=c=0.27 nm. Therefore the phase of the precipitate is cubic with a=0.27 nm. Bonfield and Edwards [10] termed the phase γI, with a=0.27 nm and the orientation I with the matrix. However, the determination of the orientation relationship and lattice parameter was performed from analyses of SADPs obtained using the electron beam parallel to a $<110>_\alpha$ direction alone.

On the other hand, lamellar precipitates after prolonged aging between 300 and 400 ˚C showed the Kurdjumov–Sachs orientation relationship to the matrix, as exemplified in Fig. 4(b). That is,

$$[011]_\alpha // [\bar{1}1\bar{1}]_\gamma;\ (\bar{1}1\bar{1})_\alpha//(110)_\gamma.$$

According to the SADP in Fig. 4(b), the lamellar precipitates in Fig. 4(a) are the equilibrium γ phase with the B2 structure and lattice parameter a=0.27 nm. Rioja and Laughlin [13] have observed the Kurdjumov–Sachs orientation when the γ phase forms directly from the supersaturated matrix.

The two γ precipitates in Fig. 1(a) have a nearly identical facet of habit plane in grain A to which they have the orientation relationship I. The orientation of the habit plane was determined by tilting the precipitates until the facet habit plane was accurately edge-on. It is given by point X_h on the stereographic projection in Fig. 1(d). The habit plane is nearly parallel to the $(\bar{2}1\bar{1})_\alpha$ plane, which is close to the $\{225\}_\alpha$ habit planes reported by Baumann *et*

al [9]. Another habit plane nearly parallel to a $\{445\}_\alpha$ plane was rarely observed, as shown in Fig. 2(a). The habit plane of plate-like γ precipitates left behind the advancing boundary was the $\{225\}_\alpha$ plane, as exemplified in Fig. 5, although the γ precipitates had the same orientation I with the Cu matrix as the boundary γ precipitates. Comparison of Fig. 5 with Fig. 3 (a) confirms that the γ precipitates are plate shaped. The $\{112\}_\alpha$ or $\{445\}_\alpha$ habit plane of the boundary γ precipitates and the $\{225\}_\alpha$ habit plane of the plate-like precipitates were universally observed on aging between 300 and 400 ˚C. On prolonged aging at these temperatures, the habit plane of lamellar precipitates was found to be $(\bar{1}1\bar{1})_\alpha$ ($//(110)_\gamma$), as shown in Fig. 4(a). This type of habit plane has been reported when the γ phase forms directly from the supersaturated matrix [13], and in Cu–6wt%Be pearlite [17].

It should be noted in Fig. 1(d) that the observed $(\bar{2}1\bar{1})_\alpha$ habit plane makes the smallest angle to the boundary plane among the 24 possible $\{112\}_\alpha$ planes (two grains). This tendency is also seen in Fig. 2(c). The precipitates have the $(\bar{5}4\bar{4})_\alpha$ habit plane second closest to the grain boundary among the 24 possible $\{445\}_\alpha$ planes. The $(54\bar{4})_\alpha$ plane in grain B makes the smallest angle to the boundary plane. Such geometry was found to hold in the present work, leading to a conclusion that the boundary precipitates are prone to nucleate in such a fashion that their habit planes with the matrix lie as close as possible to the grain boundary. This result may be understood by the theoretical analyses of Lee and Aaronson [18, 19]. The $\{112\}_\alpha$ or $\{445\}_\alpha$ habit plane is assumed to have a low energy, although it is not understood whether atomic matching at the habit plane is good. The precipitate morphology suggests that the shape of the critical nuclei of the precipitates may consist of two abutting spherical caps, one of which is truncated by the low-energy plane. Lee and Arronson have demonstrated that the ratio of the activation energy for the nucleation of a faceted nucleus to that of an unfaceted nucleus sharply decreases as the contact angle between the facet (low-energy plane) on the nucleus and the boundary plane decreases. Therefore, the precipitates which have a low-energy habit plane close to the boundary plane in one grain would nucleate preferentially.

Grain-boundary precipitation is complete prior to any significant boundary migration. When migration starts, as shown in Fig. 2(a), the boundary moves locally between two

existing γ precipitates, leaving the precipitates embedded in the grain with which they had the $\{112\}_\alpha$ or $\{445\}_\alpha$ habit plane of a low energy. A similar observation has been made in Cu–Be alloys using TEM by Baumann *et al*. [9]. It should be noted, however, that the existence of a low-energy habit plane has not been directly revealed in Figs. 3 and 7 of their paper. Also the above behavior is similar to that predicted by Tu and Turnbull [11, 12]. As pointed out by Baumann *et al*., however, there is a clear sequential difference between the process observed using TEM and the optical observations of Tu and Turnbull in Pb–Sn alloy bicrystals. In the pucker mechanism proposed by Tu and Turnbull, only one boundary precipitate is initially required to generate a whole cell of DP, whereas in the Cu–Be alloys the sequence is reversed.

The pucker mechanism for DP begins with the nucleation, on one side of the grain boundary, of a disc or plate-shaped precipitate having a high-energy interface across the grain boundary and a low-energy interface with the grain in which it is embedded. The interface energy imbalance between the two broad faces of the precipitate can be eliminated by the migration of the grain boundary along the high-energy interface, leaving the precipitate completely embedded in the grain. The difference between the interface energies produces a driving force for the boundary migration which replaces the high-energy interface by the low-energy interface. The result of Fig. 2(a) supports this idea. Most of the precipitates in Fig. 2(a) posses the $(\bar{5}4\bar{4})_\alpha$ habit plane of a low energy with the grain A alone, whereas on the far left side of Fig. 2(a), there is the habit plane on both sides of the precipitates behind the advancing boundary.

In Figs. 1 and 2, a single variant of the γ precipitates forms on the grain boundary. In general, the flat boundaries examined had a single or two variants of the γ precipitates, and one of the two variants exhibited the orientation relationship to one of the abutting grains and the other variant to the other grain. As exemplified in Fig. 2(a), on aging at 300, 325 and 350 ˚C, the grain boundaries with a single variant tended to move toward the grain opposite to the one in which the precipitates had the $\{112\}_\alpha$ or $\{445\}_\alpha$ habit plane. When there existed two variants on the boundary, the boundary was apt to move toward the grain opposite to the one to which the larger number of precipitates had the orientation relationship. Since optical

microscopy observations revealed that the growth of DP cells at flat boundaries took place in one direction only, the migration direction of the boundaries observed by TEM should determine the growth direction of cells observed by optical microscopy. On the other hand, the boundary migration on aging at 400˚C was often observed to be toward the grain in which the precipitates had the low-energy habit plane, when the boundary had a single variant of the precipitates. An example is shown in Fig. 6, where the precipitates labeled O, P and Q exhibited the orientation relationship I to the Cu matrix of grain B. As revealed in Fig. 5, boundary γ precipitates on aging at 400˚C were large and their densities were low. In this case the driving force for boundary migration cannot be attributed to the interface energy decrease. Fournelle and Clark [20] have considered that DP in Cu–In alloys can develop from an initially precipitate-free grain boundary, and boundary migration due to recrystallization and/or grain growth forces initiates the DP reaction. Given that the present specimens were fully solution treated, it seems that the grain growth is responsible for the initial boundary migration.

3. 2. Variation in cell formation and growth with the misorientation

The continuous precipitation of γ", γ' or γ phase occurred during aging at temperatures between 300 and 400˚C. However, the cell growth rate of DP was unchanged and linear in spite of the formation of γ", γ′ or γ. This is in agreement with the result of our previous work [2, 3].

Fig. 7 shows the cell width L against aging time t for 16˚ and 51˚ [011] and 18˚ and 53˚ [001] symmetric tilt boundaries in bicrystals aged at 400˚C. The data for the [001] tilt boundaries are taken from our previous study [2]. A linear relationship exists between L and t for these boundaries. For all boundaries and aging temperatures examined, L–t plots maintained such linearity. It is noted that the cell growth rates v for the [011] tilt boundaries are slower than those for the [001] tilt boundaries. This generally held. From the slope of the straight line drawn by the least-squares method, v was obtained for each boundary and aging temperature. In Fig. 8, the calculated values of v at 400˚C are given as a function of the

misorientation angle θ. The value of v depends strongly on θ. The variation of v with θ at other temperatures showed a similar tendency. It is also seen from Fig. 7 that the incubation periods τ to initiate DP (i.e. the intercept on the abscissa at L=0) at the [011] tilt boundaries are much longer than those at the [001] tilt boundaries. This tendency was generally observed. That is, the DP cells at the [001] symmetric tilt boundaries nucleate more rapidly than those at the [011] tilt boundaries. Fig. 9 shows a plot of τ at 400˚C against θ. The dependence of τ on θ is non-monotonic.

The v–θ and τ–θ curves show local cusps and peaks near θ=70.5˚ (Σ3) and θ=129.5˚ (Σ11). However, no cusps and peaks are observed at misorientation angles corresponding to the other low-Σ boundaries, e.g. θ=109.5˚ (Σ3) and θ=50.5˚ (Σ11). Such boundaries can be expected to show cusps and peaks according to the criterion of the Σ value [21], which well defines the character of grain boundaries. That is, the criterion does not explain sufficiently the existence of the observed cusps and peaks. On the other hand, the positions of the cusps and peaks in Figs. 8 and 9 are in agreement with those of deep cusps in the grain-boundary energy γ–θ curve for Cu reported by Miura *et al*. [22], although in addition to these deep cusps, there is a shallow cusp near 38.9˚ (Σ9) in the γ–θ curve. Therefore, it is concluded that the formation and growth of DP cells are easier at higher-energy boundaries.

As mentioned in Section 3.1., the γ phase first precipitated at grain boundaries. Theoretically, boundary precipitation of a second phase is influenced by such factors as grain-boundary energy γ and grain-boundary diffusion. The larger these factors, the more the boundary precipitation is enhanced [23]. No significant difference between the values of γ of [011] [22] and [001] symmetric tilt boundaries [24] can be found. Biscondi [25] has reported, however, that diffusion of Zn along Al [001] symmetric tilt boundaries is faster than along [011] tilt boundaries. A similar observation has also been made from an investigation of the diffusivity of Bi along grain boundaries in Cu bicrystals [26, 27]. Furthermore, the growth of DP cells in the present alloy can be considered to be controlled by the diffusion of Be atoms along grain boundaries, as will be described later. It may thus be expected that the nucleation and growth of DP cells are more difficult at [011] symmetric tilt boundaries than at [001] tilt boundaries. This is actually the case in the present study, as described above.

3.3. Growth Kinetics

In the literature [1], several kinetic methods are available to estimate the grain boundary diffusivity triple product, $s\delta D_b$ (where s, δ and D_b are the segregation factor, boundary thickness and boundary diffusion coefficient, respectively) through the kinetic analysis of DP using the experimentally determined kinetic parameters of v and λ. Following our previous studies [2, 3], kinetic analyses of DP in the present study have been confined to utilizing the models of Turnbull (T) [4] and Petermann and Hornbogen (P–H) [5]. The equation of T on DP is written as

$$s\delta D_b = \frac{x_0}{x_0 - x_e} v\lambda^2 \qquad [1]$$

where x_0 and x_e are the initial solute content in the alloy and the equilibrium solute content in the α phase, respectively. Values of x_e are readily obtained from the relevant equilibrium diagram [28]. The equation of P–H is expressed as follows

$$s\delta D_b = \frac{RT}{-8\Delta G} v\lambda^2 \qquad [2]$$

where R is the gas constant, and ΔG is the driving force for DP in terms of the overall change in the Gibbs energy, which is described by

$$\Delta G = -RT\left[x_0 \ln\frac{x_0}{x_e} + (1 - x_0)\ln\frac{1 - x_0}{1 - x_e}\right] + \frac{2\sigma V_m}{\lambda} \qquad [3]$$

The first term represents the chemical free energy available for the growth of DP cells (assuming ideal solution behavior [1]). The second term is associated with the free enthalpy needed for the creation of the interphase boundaries. Here σ is the interface energy of the α–γ interface which is assumed to be 0.4J/m^2 [7] and V_m is the molar volume of the initial solid solution (7.0×10^{-6} m^3/mol [29]).

Fig. 10 presents the Arrhenius plots of the respective sets of $s\delta D_b$ data derived using the models of T and P–H for a 39° boundary as a function of the reciprocal temperature. The pre-exponential factor $(s\delta D_b)_0$ and activation energy Q_b of grain-boundary diffusion were determined from the intercept and slope of the straight lines fitted to the $s\delta D_b$ data,

respectively.

Fig. 11 summarizes the values of Q_b for all the boundaries examined. For the two models, the values of Q_b depend on the misorientation. The values obtained using the T model range from 1.3 to 1.6 eV. The values determined from the P–H model are larger. The Q_b values are generally larger than those previously obtained for the [001] symmetric tilt boundaries [2]. This is coincident with the result reported by Biscondi [25] that diffusion of Zn along Al [001] symmetric tilt boundaries is faster than along [011] tilt boundaries. Since the Q_b values in this work are much smaller than the activation energy (2.03 eV [30]) of volume diffusion of Be in Cu, it can be concluded that the boundary diffusion of Be in Cu is the rate-controlling step for the cell growth.

The dependence of Q_b on θ in Fig. 11 is very analogous to the dependence of the diffusivity of Zn in Al [011] symmetric tilt boundaries reported by Biscondi [25]. Both the boundary diffusivity–θ and Q_b–θ curves exhibit cusps at θ=70.5° (Σ3) and θ=129.5° (Σ11). The positions of the peaks are in agreement with those of the energy cusps of the [011] symmetric tilt boundaries in Cu reported by Miura *et al*. [22]. Thus, we conclude that the lower the boundary energy, the lower is the boundary diffusivity.

The calculated values of $(s\delta D_b)_0$ were plotted against the misorientation. These values were generally larger than those obtained for the [001] symmetric tilt boundaries [2]. Comparison with Fig. 11 revealed that, for the two models, the larger the Q_b value, the larger is the $(s\delta D_b)_0$ value. This result is in accordance with that of the previous studies [2, 3].

4. Conclusions

Investigations on the initiation and growth of Discontinuous precipitation (DP) reaction at [011] symmetric tilt boundaries in Cu–0.75 wt % Be alloy bicrystals in the temperature range from 300 to 400 °C have yielded the following conclusions.

1. In the initiation of DP, precipitation of the γ phase occurs first at grain boundaries and then the boundaries migrate. It is found that γ precipitates are apt to form at the boundary in such a fashion that the observed $\{112\}_\alpha$ or $\{445\}_\alpha$ habit plane between the γ precipitates and one of

the grains makes an angle as small as possible to the boundary.

2. Initial boundary migration occurs locally between two existing γ precipitates, leaving the precipitates embedded in the grain in which the habit plane with a low interface energy forms on both sides of the precipitates. This behavior supports the idea of Tu and Turnbull [11, 12] that the driving force for initial boundary migration is provided by the reduction in total interface energy of a boundary precipitate.

3. The formation and growth of DP at [001] symmetric tilt boundaries in bicrystals of the same alloy take place more easily compared with those at [011] symmetric tilt boundaries. Both the incubation period for cell formation and the cell growth rate at a boundary exhibit a good correlation with the energy of the boundary. That is, lower-energy boundaries have a longer incubation period and a slower growth rate.

4. The grain-boundary diffusion data have been determined through the kinetic analysis of DP using the models of Turnbull [4] and Petermann and Hornbogen [5]. A close correlation is found between the diffusivity and the energy of boundaries. The higher the boundary energy, the more easily the boundary diffusion occurs with a smaller activation energy and a smaller pre-exponential factor.

ACKNOWLEDGEMENT

We acknowledge Mr. Higashimine of Center for Nano Materials and Technology, Japan Advanced Institute Science and Technology, for the TEM observation.

REFERENCES

[1] Manna I, Pabi SK, Gust W. Inter Mater Rev 2001;46:53.

[2] Monzen R, Shigehara H, Kita K. J Mater Sci 2000;35:5839.

[3] Monzen R, Kita K, Shigehara H. Met Mater Trans A 2001;32A:1075.

[4] Turnbull D. Acta Metall 1955;3:55.

[5] Petermann J, Hornbogen E. Z Metallk 1968;59:814.

[6] Borchers H, Schulz H. Acta Metall 1976;24:639.

[7] Tsubakino H, Nozato R. J. Jpn Inst Metals 1979;43:42.

[8] Tsubakino H, Nozato R, Hagiwara H. Trans Jpn Inst Metals 1981;22:153.

[9] Baumann SF, Michael J, Williams DB. Acta Metall 1981;29:1343.

[10] Bonfield W, Edwards BC. J Mater Sci 1974;9:409.

[11] Tu KN, Turnbull D. Acta Metall 1967;15:369.

[12] Tu KN, Turnbull D. Acta Metall 1967;15:1317.

[13] Rioja RJ, Laughlin DE. Acta Metall 1980;28:1301.

[14] Tsubakino H, Nozato R, Yamamoto A. Mater Sci Tech 1993;9:288.

[15] Shimizu K, Mikami Y, Mitani H, Otsuka K. Trans Jpn Inst Metals 1971;12:206.

[16] Geisler AH, Mallery J, Steigert FE. J Metals 1952;4:307.

[17] Beatty JH, Hackney SA, Shiflet GJ. Philos Mag A 1988;57:457.

[18] Lee JK, Aaronson HI. Acta Metall 1975;23:799.

[19] Lee JK, Aaronson HI. Acta Metall 1975;23:809.

[20] Fournelle RA, Clark JB. Metall Trans A 1972;3:2757.

[21] Brandon DG, Ralph B, Ranganathan S, Wald MS. Acta Metall 1964;12:813.

[22] Miura H, Kato M, Mori T. J Phys 1990;51:C1-263.

[23] Turnbull D. Solid State Phys 1956;3:225.

[24] Mori T, Ishii T, Kajihara M, Kato M. Philos Mag Lett 1997;75:367.

[25] Biscondi M. Physical Chemistry of the Solid States: Applications to Metals and their Compounds, in: Lacombe P. editor. Amsterdam: Elsevier; 1984. p. 225.

[26] Monzen R, Okamoto T. Mater Sci forum 1999;294-296:561.

[27] Monzen R, Kuze T. J Jpn Inst Metals 1999;63:1224.

[28] Binary Alloy Phase Diagrams, ASM International, In: Massalski TB, *et al.*, editors. Materials Park (OH): ASM International, 1992. p. 645.

[29] Tanimura H, Wassermann G. Z Metallk 1933;25:179.

[30] Fogel'son RL, Ugay YA, Pokoyev AV, Akimova IA, Kretinin VD. Phys Metall Metallogr 1973;35:176.

Figure Captions

Fig. 1. (a) TEM image of γ precipitates at a θ=130˚ boundary in a bicrystal aged at 400˚C for 60 h. The precipitates have the $(\bar{2}1\bar{1})_\alpha$ habit plane in grain A. (b) $[011]_\alpha$ selected-area diffraction pattern (SADP) corresponding to (a). (c) Schematic illustration of the previous SADP. (d) $(011)_\alpha$ stereographic projection corresponding to (a).

Fig. 2. (a) TEM image of γ precipitates at a θ=153˚ boundary in a bicrystal aged at 325˚C for 120 h. The precipitates have the $(\bar{5}4\bar{4})_\alpha$ habit plane in grain A. The boundary bows out between the neighboring γ precipitates. (b) $[011]_\alpha$ SADP corresponding to (a). (c) $(011)_\alpha$ stereographic projection corresponding to (a).

Fig. 3. (a) TEM image of a plate-shaped γ precipitate left behind a θ=51˚ boundary advancing after aging at 400˚C for 84 h. (b) $[100]_\gamma$ SADP corresponding to (a). (c) Stereographic projection corresponding to (a).

Fig. 4. (a) TEM image of lamellar precipitates behind a θ=51˚ boundary advancing in a bicrystal aged at 400˚C for 336 h. The precipitates have the $(\bar{1}1\bar{1})_\alpha$ habit plane parallel to $(110)_\gamma$. (b) [011] SADP corresponding to (a).

Fig. 5. TEM image of plate-shaped γ precipitates left behind a θ=51˚ boundary advancing in a bicrystal aged at 400˚C for 84 h. The precipitates have the $(\bar{5}2\bar{2})_\alpha$ habit plane. The zone axis is $[011]_\alpha$.

Fig. 6. TEM image showing the movement of a θ=39˚ boundary in a bicrystal aged at 400˚C for 48 h, leaving a precipitate O behind the boundary.

Fig. 7. Change in the cell width L with aging time t for 16˚ and 51˚ [011] and 18˚ and 53˚ [001] symmetric boundaries in bicrystals aged at 400˚C.

Fig. 8. Cell growth velocity v at 400˚C, plotted against the misorientation angle θ for [011] symmetric tilt boundaries.

Fig. 9. Incubation period τ to initiate DP at 400˚C, plotted against the misorientation angle θ for [011] symmetric tilt boundaries.

Fig. 10. Arrhenius plots of the $s\delta D_b$ values obtained using the Turnbull (T) and Petermann and Hornbogen (P–H) models for a 39˚ boundary.

Fig. 11. Activation energy Q_b values for grain-boundary diffusion obtained using the T and P–H models, plotted against the misorientation angle θ for [011] symmetric tilt boundaries.

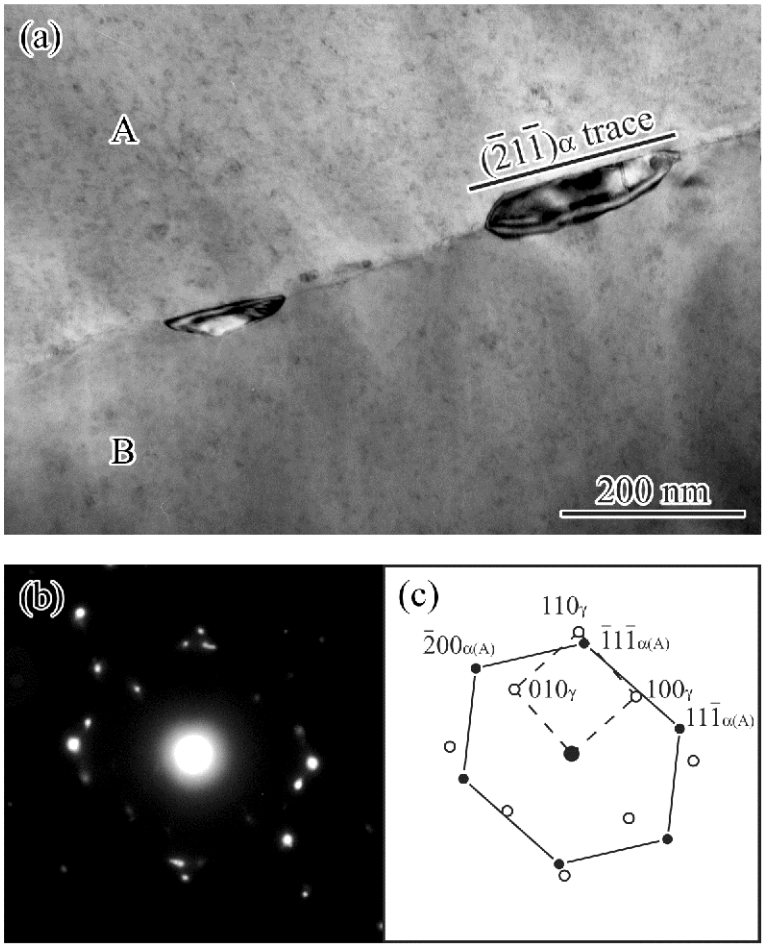

Fig. 1(a), (b) and (c)
Monzen *et al.*

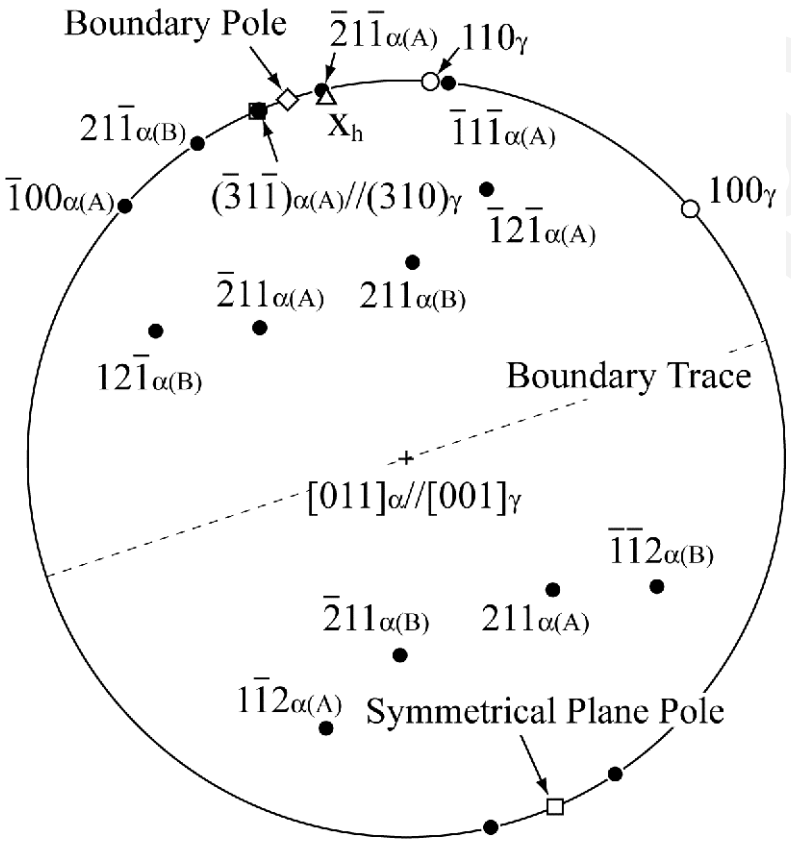

Fig. 1(d)

Monzen *et al.*

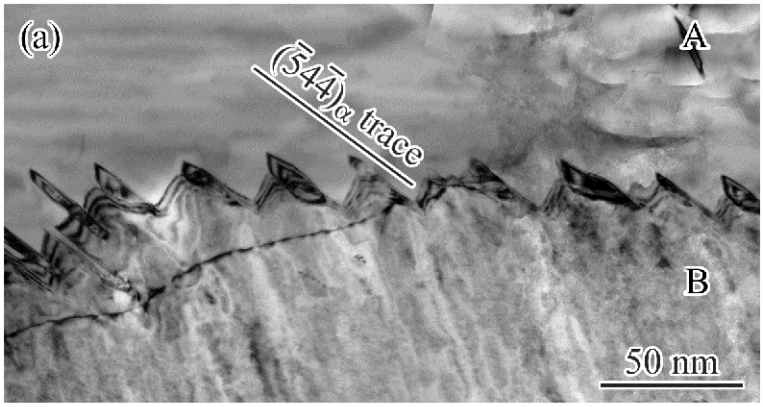

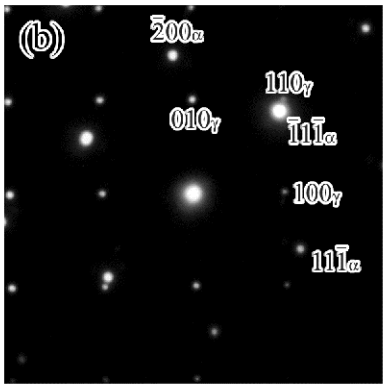

Fig. 2(a) and (b)
Monzen *et al.*

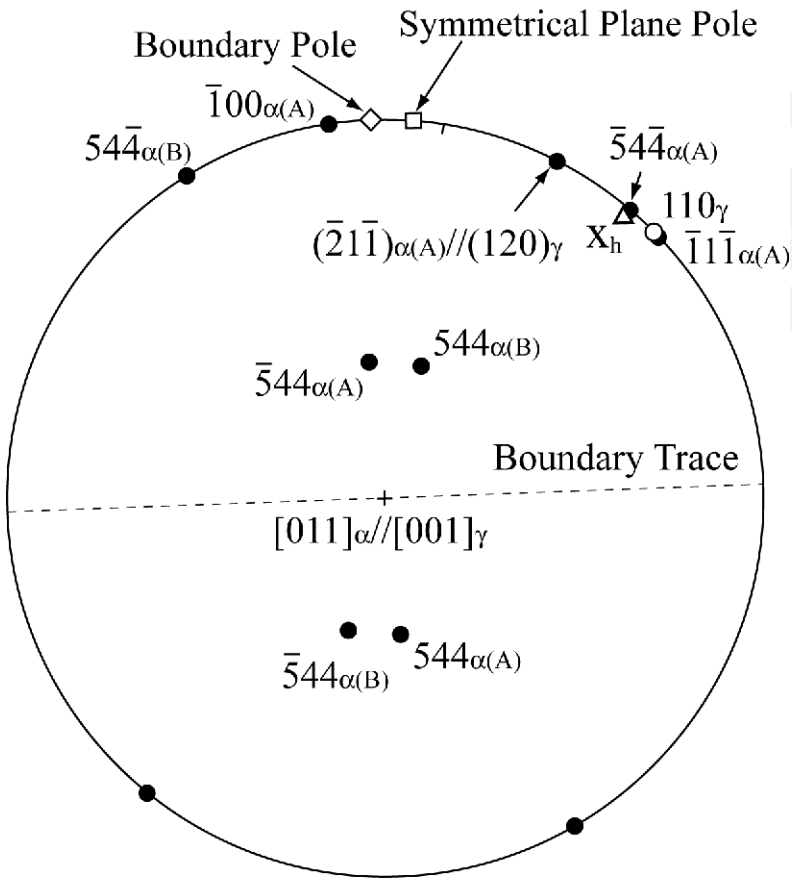

Fig. 2(c)

Monzen *et al.*

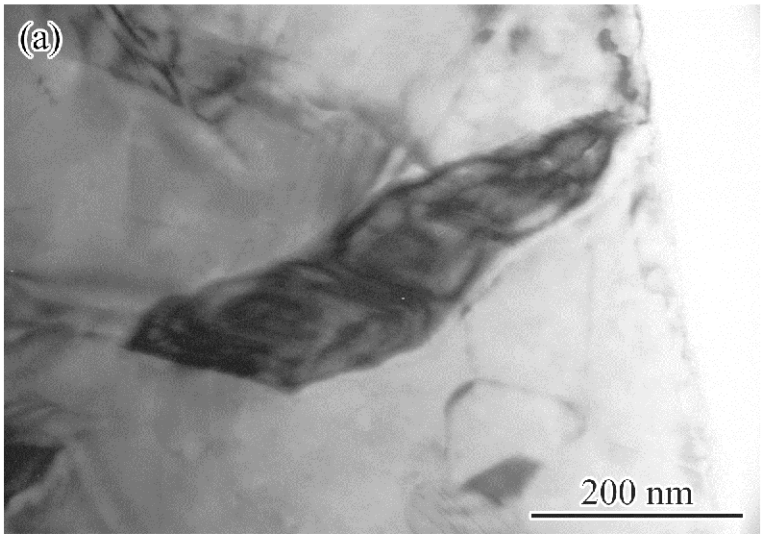

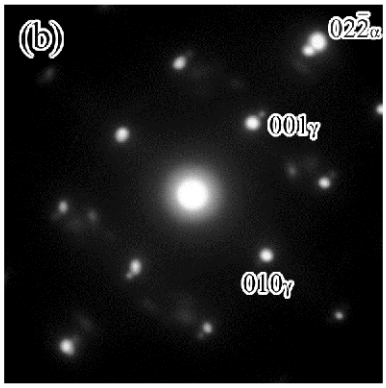

Fig. 3(a) and (b)
Monzen *et al.*

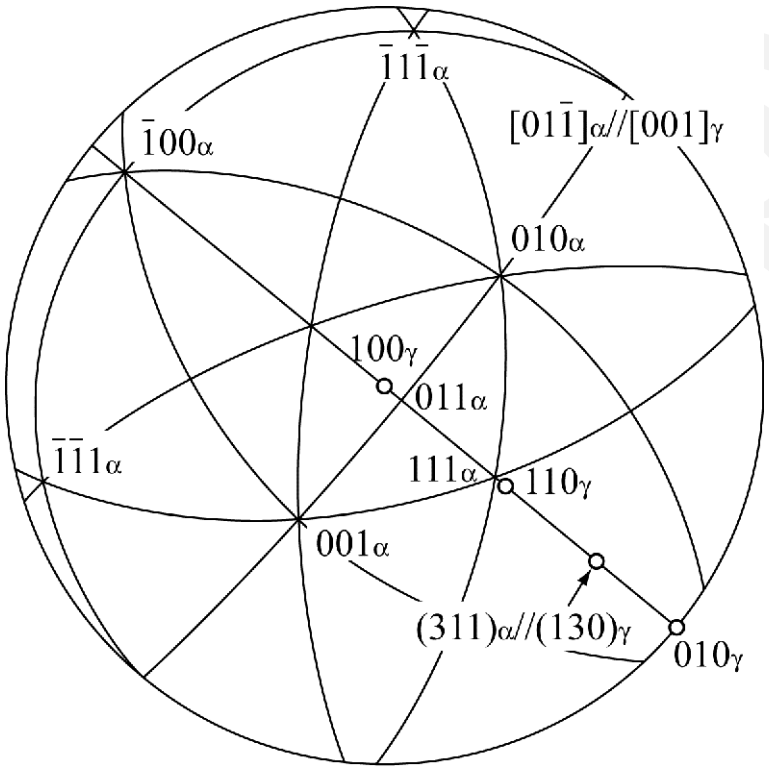

Fig. 3(c)

Monzen *et al.*

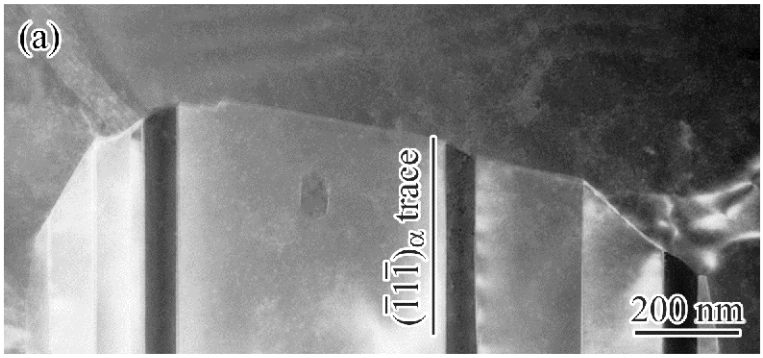

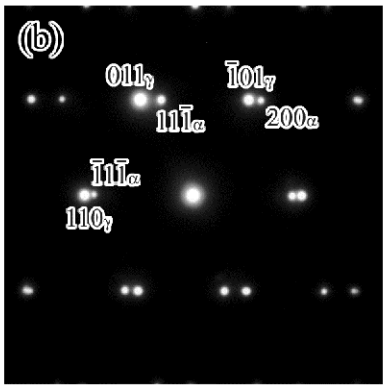

Fig. 4(a) and (b)

Monzen *et al.*

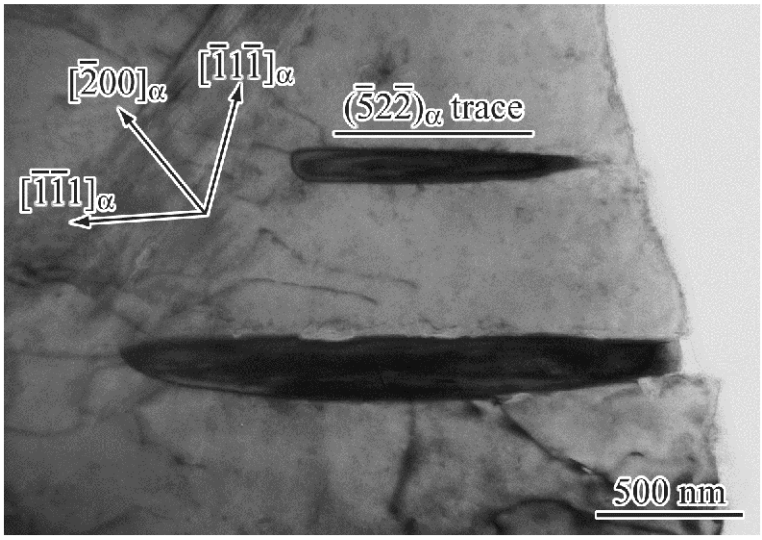

Fig. 5

Monzen *et al.*

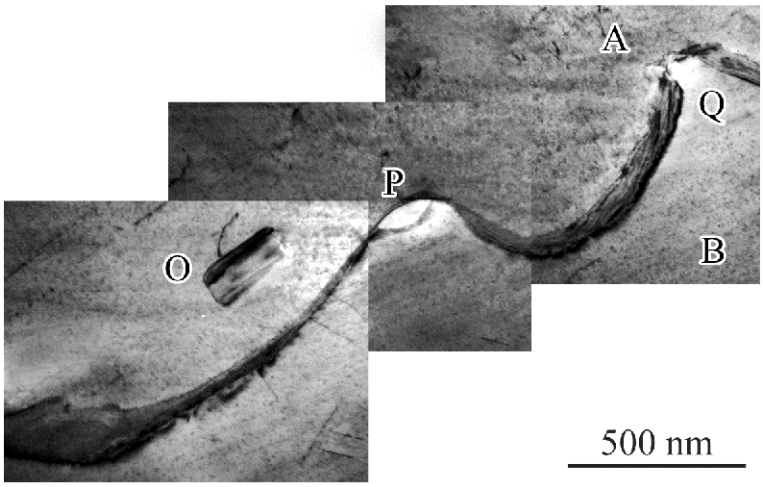

Fig. 6

Monzen *et al.*

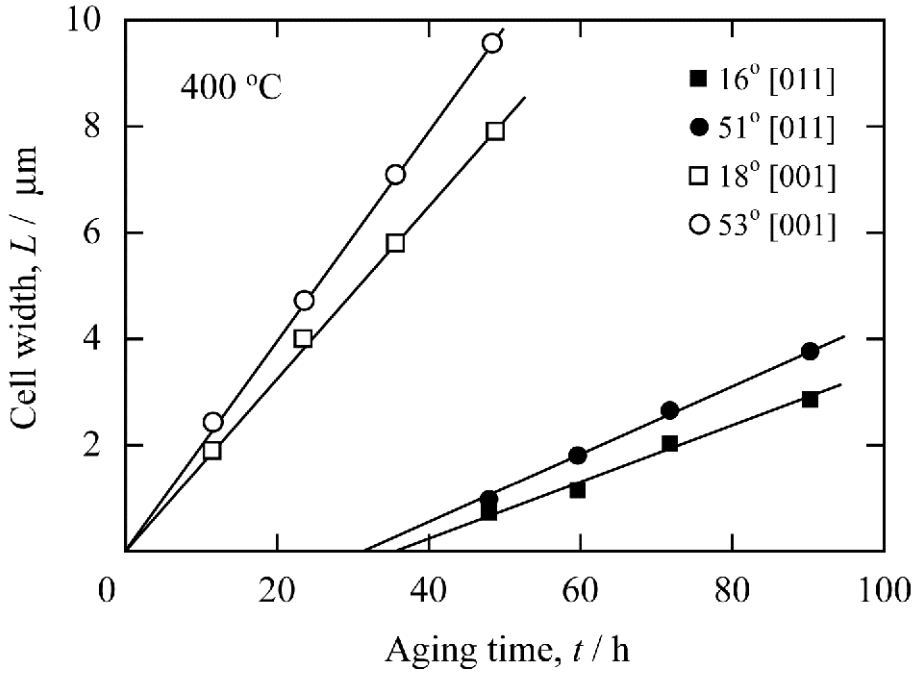

Fig. 7

Monzen *et al.*

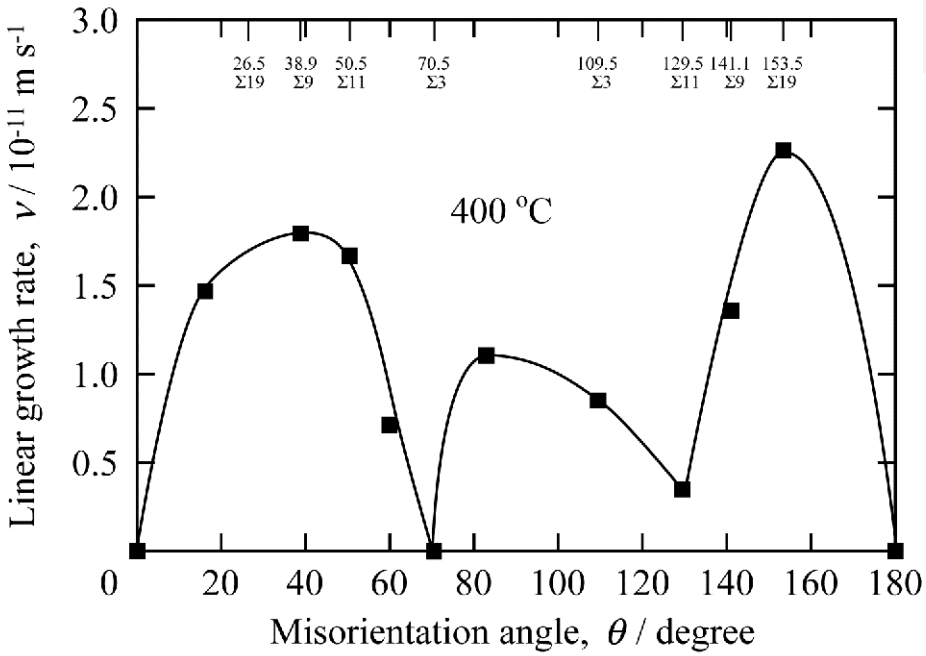

Fig. 8

Monzen *et al.*

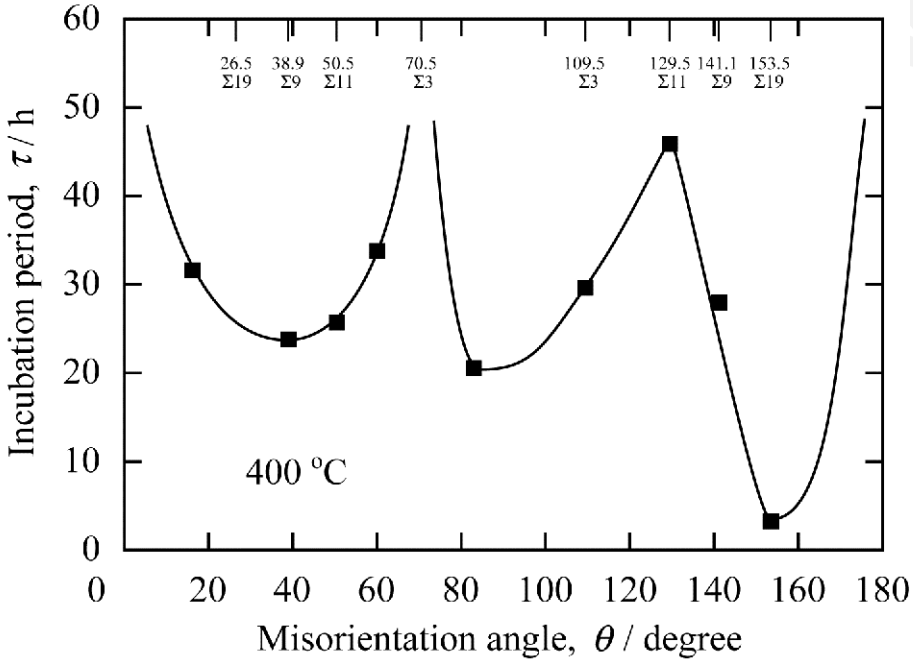

Fig. 9

Monzen *et al.*

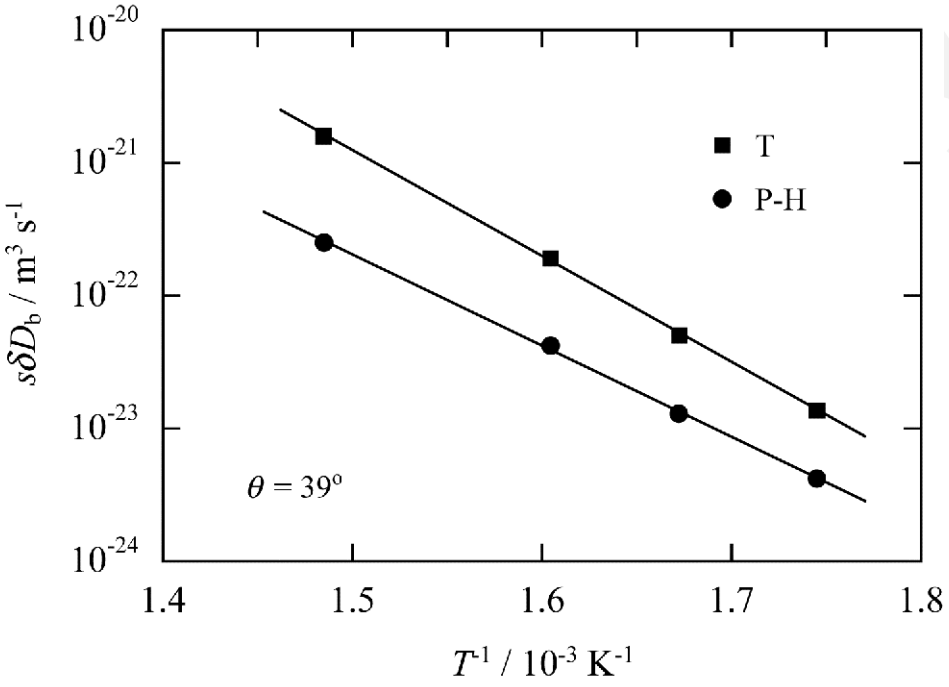

Fig. 10

Monzen *et al.*

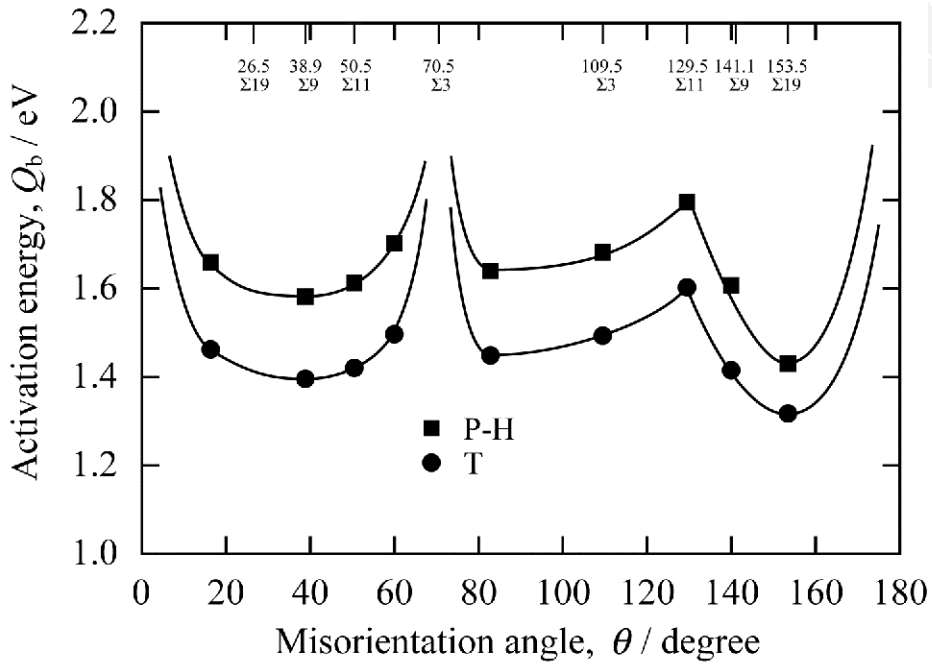

Fig. 11.

Monzen *et al.*